THE JOURNAL OF BIOLOGICAL CHEMISTRY VOL. 285, NO. 45, pp. 35188–35195, November 5, 2010

The Anti-inflammatory Drug Indomethacin Alters Nanoclustering in Synthetic and Cell Plasma Membranes*

Received for publication, May 4, 2010, and in revised form, August 23, 2010 Published, JBC Papers in Press, September 7, 2010, DOI 10.1074/jbc.M110.141200

Yong Zhou, Sarah J. Plowman, Lenard M. Lichtenberger[1], and John F. Hancock[2]

From the Department of Integrative Biology and Pharmacology, The University of Texas Medical School at Houston, Houston, Texas 77030

The nonsteroidal anti-inflammatory drug indomethacin exhibits diverse biological effects, many of which have no clear molecular mechanism. Membrane-bound receptors and enzymes are sensitive to their phospholipid microenvironment. Amphipathic indomethacin could therefore potentially modulate cell signaling by changing membrane properties. Here we examined the effect of indomethacin on membrane lateral heterogeneity. Fluorescence lifetime imaging of cells expressing lipid-anchored probes revealed that treatment of BHK cells with therapeutic levels of indomethacin enhances cholesterol-dependent nanoclustering, but not cholesterol-independent nanoclustering. Immuno-electron microscopy and quantitative spatial mapping of intact plasma membrane sheets similarly showed a selective effect of indomethacin on promoting cholesterol-dependent, but not cholesterol-independent, nanoclustering. To further evaluate the biophysical effects of indomethacin, we measured fluorescence polarization of the phase-sensitive probe Laurdan and FRET between phase-partitioning probes in model bilayers. Therapeutic levels of indomethacin enhanced phase seperation in DPPC/DOPC/Chol (1:1:1) and DPPC/Chol membranes in a temperature-dependent manner, but had minimal effect on the phase behavior of pure DOPC at any temperature. Taken together, the imaging results on intact epithelial cells and the biophysical assays of model membranes suggest that indomethacin can enhance phase separation and stabilize cholesterol-dependent nanoclusters in biological membranes. These effects on membrane lateral heterogeneity may have significant consequences for cell signaling cascades that are assembled on the plasma membrane.

Non-steroidal anti-inflammatory drugs (NSAIDs)[3] are widely used for their anti-inflammatory, analgesic, and antipyretic effects. Long-term administration of NSAIDs has also been reported to prevent the progression of various types of cancer (colon, gastric, esophageal, pulmonary, prostate, ovarian, and breast); cardiovascular disease (myocardial infarction, thrombosis, and stroke); diabetes (insulin-resistant and related metabolic syndrome); and diseases of the peripheral and central nervous system (Alzheimer disease, Parkinson) (1). Despite the increased usage of NSAIDs over the past decades (1), the molecular basis for these diverse biological activities is not fully understood.

The cyclooxygenase (COX) inhibitory activities of NSAIDs contribute to their anti-inflammatory, analgesic, and antipyretic effects, as well as gastrointestinal side effects (1). However, many biological activities of NSAIDs are COX-independent, including their effects on amyloidogenic Aβ42 production (2), tight junctions (3), neutrophil adhesion, and transmigration (3), and cell apoptosis and proliferation (4). Whereas it is possible that NSAIDs interact with multiple protein targets, it is quite feasible that these drugs influence cell function by a more general mechanism. NSAIDs are amphiphilic, are capable of strong association with phospholipids (5, 6) and possess large membrane partition coefficients (7). At the high concentrations found in the gastrointestinal tract NSAIDS disrupt a phospholipid monolayer covering the gastric mucus layer, contributing to gastric injury (6). NSAIDs also perturb membrane integrity resulting in altered red blood cell morphology (8) and reduced mechanical stability of phosphatidylcholine (PC) membranes (5). Other amphiphilic drugs, such as local and general anesthetics, influence membrane biophysical properties which contribute, in part, to their diverse biological activities (9). Extrapolating from these studies we hypothesize that NSAIDs intercalate in cell membranes and by perturbing lipid-lipid interactions modulate diverse membrane-scaffolded biological processes. Nanoclustering in biological membranes is related to phase separation in synthetic model membranes and reflects changes in the lateral packing of phospholipids that may cause changes in the structure, localization, and function of membrane proteins (10–13). We therefore examined whether a potent NSAID, indomethacin, alters nanoclustering in baby hamster kidney cell plasma membrane. The outcome of this *in vivo* study was then correlated to the effect of indomethacin on phase behavior in model liposomes. To the best of our knowledge, the concept that NSAIDs may have broad effects on cell function by changing membrane domain organization has not previously been examined. The studies we describe here provide strong preliminary evidence in favor of this proposal.

* This work was supported, in whole or in part, by National Institutes of Health Grants F-32 DK07664 and R01 GM066717 and the Texas Medical Center Digestive Disease Center PHS P-30DK56338.

[1] To whom correspondence may be addressed: 6431 Fannin St., MSB 4.098, Houston, TX 77030. Tel.: 713-500-6320; E-mail: lenard.m.lichtenberger@uth.tmc.edu.

[2] Current incumbent of the Fondren Chair in Cellular Signaling. To whom correspondence may be addressed. Tel.: 713-500-7547; E-mail: john.f.hancock@uth.tmc.edu.

[3] The abbreviations used are: NSAID, non-steroidal anti-inflammatory drug; Indo, indomethacin; DPPC, dipalmitoyl phosphatidylcholine; DOPC, dioleoyl phosphatidylcholine; (DPPE)-NBD, dipalmitoyl phosphatidylethanolamine-7-nitrobenz-2-oxa-l,3-diazol-4-yl; (DOPE)-NBD, dioleoyl phosphatidylethanolamine; Chol, cholesterol; L_o, liquid-ordered domains; L_d, liquid-disordered domains; FLIM, fluorescence lifetime imaging microscopy; EM, electron microscopy; GP, generalized polarization; LUV, large unilamellar vesicles; PFA, paraformaldehyde.

EXPERIMENTAL PROCEDURES

Materials—Dipalmitoyl phosphatidylcholine (DPPC), dioleoyl phosphatidylcholine (DOPC), dipalmitoyl phosphatidylethanolamine-7-nitrobenz-2-oxa-l,3-diazol-4-yl (DPPE)-NBD, dioleoyl phosphatidylethanolamine (DOPE)-NBD, and (DOPE)-rhodamine were purchased from Avanti Polar Lipids, Inc. (Alabaster, AL). Lipids were dissolved in chloroform and stored at −20 °C under nitrogen. Cholesterol was purchased from Sigma-Aldrich and 6-dodecanoyl-2-dimethylaminonaphthalene (Laurdan) was purchased from Molecular Probes (Carlsbad, CA).

Indomethacin was first dissolved in PBS to make a 50 mM stock solution. Because indomethacin is not easily solubilized in aqueous solution, we slowly increased the pH of the PBS solution (maintaining the solution pH < 9) while providing minimal heating (< 38 °C). Once all indomethacin dissolved, the pH was then slowly adjusted back down to ~7.4. The concentration of indomethacin was checked by HPLC.

Fluorescence Lifetime-imaging Microscopy-FRET (FLIM-FRET)—Expression vectors for GFP-tH, RFP-tH, GFP-tK, and RFP-tK have been described previously (14–16). Each construct comprises mGFP or mRFP appended with the C-terminal minimal membrane anchors of H-Ras (-tH) or K-Ras (-tK), respectively. Baby Hamster Kidney (BHK) cells cultured in DMEM containing 10% BCS were transfected using Lipofectamine according to manufacturer's instructions. Twenty-four hours after transfection, cells were treated with various concentrations of indomethacin for 1 h in serum free DMEM, then washed, and fixed with 4% paraformaldehyde (PFA). GFP lifetime was measured using a Lambert Instruments (Roden, The Netherlands) FLIM attachment on a wide field microscope. Cells expressing combinations of GFP-tH, RFP-tH, GFP-tK, and RFP-tK were excited using a sinusoidally modulated 3W 497 nm LED at 40 MHz under epi-illumination. Fluorescein was used as a lifetime reference standard (~4.1 ns). Cells were imaged with a 60x Plan-Apo/1.4 NA oil objective using an appropriate GFP filter set. The phase and modulation lifetimes were determined from a set of 12 phase settings using the manufacturer's software. Three independent experiments were performed for each treatment, and data from a total of 35–50 cells were pooled to calculate mean and S.E.

Immuno-electron Microscopy (EM) and Spatial Analysis—Immuno-EM and spatial analysis were conducted exactly as described previously (13, 17–19). In brief, BHK cells were cultured on glass coverslips to ~80% confluency and treated with 100 μM indomethacin for 1 h. Intact apical cell plasma membrane sheets were attached to EM grids, washed, and fixed in 4% PFA, 0.1% glutaraldehyde. Grids were incubated with anti-GFP antisera directly coupled to 4 nm gold, washed, stained in uranyl acetate and embedded in methylcellulose. Digital images of the immunogold-labeled plasma membrane sheets were taken at 100,000× magnification in an electron microscope. Intact 1 μm^2 areas of the plasma membrane sheet were identified and the (x,y) coordinates of each gold particle determined using Image J software. K-functions and transformations (20) were calculated according to Equations 1 and 2 and standardized on the 99% confidence interval (CI) estimated from Monte Carlo simulations,

$$K(r) = A\, n^{-2} \sum_{j \neq i} w_{ij} 1(\|x_i - x_j\| \leq r) \quad \text{(Eq. 1)}$$

$$L(r) - r = \sqrt{K(r)/\pi} - r \quad \text{(Eq. 2)}$$

where $K(r)$ is the K-function for a pattern of n points in an area A, r = radius at which $K(r)$ is calculated (here we evaluate $1 < r < 240$ nm at 1 nm increments), $\|\cdot\|$ is Euclidean distance, $1(\cdot)$ is the indicator function, this takes a value of 1 if $\|x_i - x_j\| \leq$ r and 0 otherwise, w_{ij}^{-1} is the proportion of the circumference of the circle with center x_i and radius $\|x_i - x_j\|$ contained within A, this term builds in an unbiased edge correction for points at the edge of the study area. $L(r)-r$ is a linear transformation of $K(r)$, under the null hypothesis of complete spatial randomness $L(r)-r$ has an expected value of 0 for all values of r (21, 22). Bootstrap tests to examine differences between replicated point patterns were constructed exactly as described (23) and statistical significance evaluated against 1000 bootstrap samples.

Large Unilamellar Vesicle Formation—Approximately 20 mg of PC lipids in chloroform were dried under nitrogen gas and exposed to vacuum overnight to completely evaporate chloroform. The lipid film was rehydrated with 10 ml of phosphate buffer solution (PBS) at pH 7.4 and incubated at a temperature well above the highest melting temperature in the lipid mixture under nitrogen gas for at least 30 min. Lipid solution was extruded across a polycarbonate filter with 100 nm pores in a Mini-extruder set-up (Avanti Polar Lipids, Inc) at ~66 °C to form large unilamellar vesicles (LUVs). In all experiments, liposomes were incubated for 30 min in PBS buffer containing indomethacin before measurements.

Fluorescence Resonance Energy Transfer (FRET)—The technique of FRET to characterize membrane phase separation has been well developed (24, 25). LUVs were labeled with 0.5 mol% of donor (DPPE)-NBD with or without acceptor (DOPE)-rhodamine. Fluorescence intensity of NBD in the presence or absence of acceptor DOPE-rhodamine was measured at room temperature by using QuantaMaster UV/VIS spectrofluorometer. The efficiency of energy transfer, E, was calculated as: $E = (I_D - I_{D-A})/I_D$, where I_D is NBD intensity in the sample containing only donor probe and I_{D-A} is NBD intensity in the sample with both donor and acceptor probes.

Laurdan Generalized Polarization (GP) Measurements—Generalized polarization of Laurdan has been used to determine membrane phase heterogeneity in both synthetic model membranes and biological membranes in many studies (26–35). A Laurdan molecule positions a naphthalene group near the lipid glycerol backbone with lauric acid aligned with acyl chains (36). In a polar solvent, a portion of the excited state energy of Laurdan is lost to the reorientation of solvent molecules (36). Because of this dipolar relaxation, the emission spectrum of Laurdan displays a red shift as solvent polarity increases (Fig. 1*a*). Our goal is to use Laurdan to examine the effect of indomethacin on membrane phase behavior. It was important therefore to ensure that changes in Laurdan fluorescence properties induced by indomethacin indicate alteration in membrane phase behavior and are not caused by direct interactions

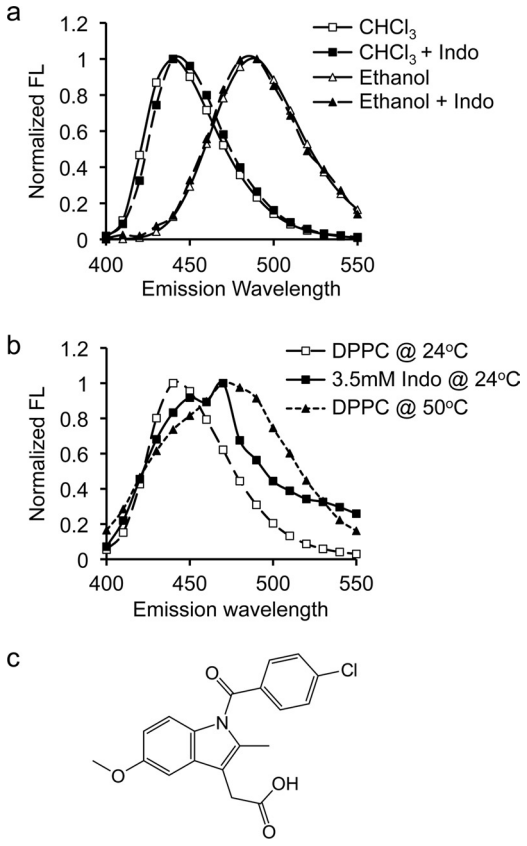

FIGURE 1. **Emission spectral shift of Laurdan in organic solvents and phospholipid bilayers.** *a*, emission spectral shift of Laurdan depends on the polarity of the surrounding environment. In non-polar chloroform (*diamonds*), Laurdan emission spectrum (excited at 340 nm) displays a peak at 440 nm. Exposure to polar ethanol (*circles*) shifts the emission spectrum to the right to 490 nm. The presence of Indo has no effect on emission spectra of Laurdan in either solvent, confirming no direct interaction between indomethacin molecules and the probe. *b*, in a phospholipid membrane, the emission spectral shift of Laurdan depends on the membrane phase behavior. The spectral peak of Laurdan in gel phase DPPC (at 24 °C) occurs at 440 nm. Increasing the temperature to 50 °C shifts the emission peak to 490 nm, indicating a transition to liquid phase. Addition of 3.5 mM indomethacin at 24 °C moves the Laurdan emission peak to a position between gel phase and liquid phase of DPPC. Two peaks are found: at ~450 nm and ~470 nm. *c*, chemical structure of indomethacin.

between indomethacin and Laurdan. To do this, we dissolved Laurdan in pure organic solvents of chloroform or ethanol, with or without indomethacin. We found that indomethacin caused no change in the Laurdan emission spectrum (Fig. 1*a*), indicating that indomethacin does not specifically interact with Laurdan and does not influence the fluorescence characteristics of the probe. Thus, changes in Laurdan fluorescence observed in this study reflect changes in membrane phase behavior.

30 ml of Laurdan (1 mg/ml stock in ethanol) was mixed with lipids in chloroform and LUVs were synthesized as described above. Emission spectra of Laurdan between 400 nm and 550 nm were obtained at various excitation wavelengths between 320 nm and 410 nm in a QuantaMaster UV/vis spectrofluorometer (Photon Technology International, Inc. Birmingham, NJ). Temperature control was achieved by utilizing a Neslab circulating chiller (Thermo Scientific, Waltham, MA) and continuously monitored by a digital thermometer. An example of emission spectrum of Laurdan in DPPC excited at 340 nm at room temperature (24 °C) is shown in Fig. 1*b*. The spectrum displays a peak at 440 nm, suggesting that the DPPC bilayer (T_m = 41 °C) is in gel phase (30). The spectrum of Laurdan in DPPC shifts to the right to 490 nm at 50 °C, confirming a liquid phase above the T_m (Fig. 1*b*). Excitation GP values are calculated by using intensity values at 440 and 490 nm in Equation 3,

$$GP = (I_{440} - I_{490})/(I_{440} + I_{490}) \quad \text{(Eq. 3)}$$

where I_{440} and I_{490} are intensity values at emission wavelengths of 440 nm and 490 nm, respectively. In a liquid phase, L_d, Laurdan displays a progressive red shift when excitation wavelength increases, because of dipolar relaxation, yielding a negative slope of the GP curve (30, 33). In a gel phase, GP is insensitive to the excitation wavelength because of a lack of solvent molecules, hence a flat GP curve. When coexisting phases are present, the fluorescent intensity of Laurdan in L_d phase gradually decreases because these molecules undergo dipolar relaxation as in the case of the pure liquid domain, while Laurdan molecules in L_o phase stay unaffected as in a pure gel phase. This means the contribution of Laurdan GP in L_o phase to the total GP becomes more dominant as the excitation wavelength increases, resulting in a gradual increase in GP and a positive slope of the GP curve.

RESULTS

Indomethacin Stabilizes Cholesterol-dependent Nanoclusters in Biological Membranes—The spatial distribution of lipid-anchored proteins on the plasma membrane is determined, in part, by the non-random distribution of lipids in the bilayer. As a general screen for effects of indomethacin on the organization of the plasma membrane we utilized fluorescence lifetime imaging microscopy (FLIM) to monitor the distribution of lipid anchored fluorescent proteins (14–16). We have shown previously that the minimal membrane anchor of H-ras (-tH) appended to GFP or RFP undergoes post-translational farnesylation and dual palmitoylation. The covalent attachment of the fully saturated palmitoyl (16:0) acyl chains to GFP targets GFP-tH to cholesterol-dependent nanoclusters on the inner leaflet of the plasma membrane (13, 17, 37, 38). GFP-tH nanoclusters have a radius of ~12 nm and contain ~7 GFP-tH molecules, or a mixture of RFP-tH and GFP-tH molecules if both fluorescent proteins are co-expressed. FRET between co-clustered donor GFP and acceptor RFP molecules results in a reduced GFP lifetime. BHK cells transiently expressing GFP-tH, with or without RFP-tH, were treated with indomethacin, and GFP lifetime was measured in single cells. The lifetime of donor GFP was ~2.15 ns in cells expressing GFP-tH alone, but was decreased to ~1.85 ns in cells co-expressing the FRET acceptor, RFP-tH, as a result of energy transfer between the probes (Fig. 2, *a* and *b*). Treatment with indomethacin at concentrations from 0.1 to 1.5 mM led to a further marked decrease ($p \ll 0.001$) in the GFP lifetime to ~1.75 ns in cells expressing both GFP-tH and RFP-tH (Fig. 2, *a* and *b*), indicating increased FRET between the probes. These indomethacin concentrations have been used in many animal (39–42) as well as human studies (43). Indomethacin had no effect on GFP lifetime in cells expressing GFP-tH alone (data not shown). We conclude that indomethacin increases the extent of GFP-tH RFP-tH

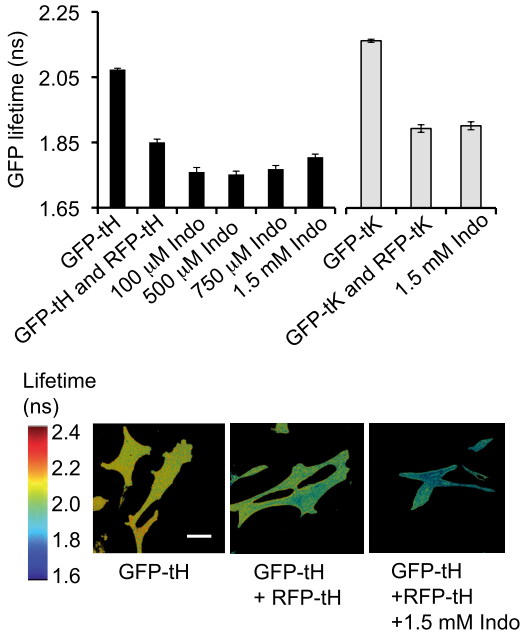

FIGURE 2. **Effect of indomethacin on nanoclusters in epithelial cell plasma membrane.** The lifetime of GFP in BHK cells expressing GFP-tH or GFP-tK alone, or coexpressing GFP-tH and RFP-tH, or GFP-tK and RFP-tK, in the presence or absence of indomethacin, was measured in a wide field FLIM microscope. Data were collected from multiple single cells. GFP lifetime is shown as mean ± S.E. (n = 50–100 cells from three independent experiments). Significant differences are indicated (*, p ≪0.05; $p = 8.6 \times 10^{-5}$ for 100 μM indomethacin, $p = 0.00014$ for 500 μM indomethacin, $p = 0.018$ for 750 μM indomethacin and $p = 4.2 \times 10^{-11}$ for 1.5 mM indomethacin). The *lower panel* contains FLIM images from a representative experiment, showing of BHK cells expressing GFP-tH alone, or co-expressing GFP-tH and RFP-tH and treated with 1.5 mM indomethacin. Scale bar: 20 μm.

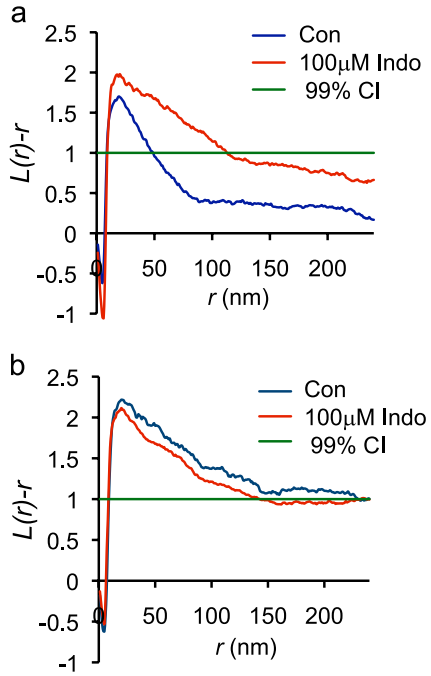

FIGURE 3. **EM analysis of GFP-tH and GFP-tK nanoclustering.** Plasma membrane sheets of BHK cells transiently expressing GFP-tH or GFP-tK, were labeled with anti-GFP-5 nm gold, imaged in an electron microscope and analyzed using spatial statistics. Plasma membrane sheets generated from BHK cells expressing GFP-tH (*a*) or GFP-tK (*b*), and left untreated or treated with 100 μM indomethacin, were labeled with anti-GFP antibody conjugated to 5 nm gold. The plasma membrane sheets were imaged in an electron microscope and the spatial distribution of the gold labeling was analyzed using Ripley's K-function (Equations 1 and 2). Maximum $L(r) - r$ values above the 99% confidence interval (C.I.) for complete spatial randomness (*CSR*) indicate clustering at that value of r. Univariate K-functions are weighted means (n = 18) standardized on the 99% C.I. Significant differences from the control pattern for indomethacin-treated cells were assessed using Bootstrap tests. Treatment with indomethacin significantly altered GFP-tH nanocluster formation ($p = 1 \times 10^{-3}$), but not GFP-tK nanocluster formation ($p = 1$).

co-clustering, consistent with either stabilization of, or increased formation of cholesterol-dependent nanoclusters in BHK cell plasma membrane.

For comparison with GFP-tH, we examined the effect of indomethacin on a subset of cholesterol-independent nanoclusters. The minimal membrane anchor of K-Ras (−tK) appended to GFP targets GFP-tK to cholesterol-independent nanoclusters on the inner plasma membrane (10–13, 17). BHK cells expressing GFP-tK with or without RFP-tK were treated with 1.5 mM indomethacin and GFP lifetime was measured. Fig. 2*a* shows that the lifetime of GFP was ~2.16 ns in cells expressing only GFP-tK and decreased to ~1.89 ns in the presence of the FRET acceptor, RFP-tK, as a result of energy transfer between the probes. Unlike the case with GFP-tH, indomethacin treatment did not further decrease the lifetime of GFP-tK, indicating that indomethacin does not alter the clustering behavior of GFP-tK in cholesterol-independent nanoclusters in the plasma membrane.

To further quantify the effect of indomethacin, plasma membrane sheets were prepared from BHK cells transiently expressing GFP-tH, labeled with anti-GFP-4 nm-gold and imaged by electron microscopy. The distribution of the immunogold point pattern was analyzed using spatial statistics. The $L(r) - r$ plot in Fig. 3*a* shows a positive deflection outside the 99% CI for a random pattern indicating that the GFP-tH immunogold point pattern is clustered. Fig. 3*a* also shows that incubation in 100 μM indomethacin induced a statistically significant increase ($p < 0.05$) in GFP-tH clustering. In contrast, indomethacin had no significant effect on the clustering of GFP-tK (Fig. 3*b*). To gain further insight into the nature of the effect of indomethacin we re-interrogated the point patterns to derive an estimate of the number of gold particles per cluster, and the fractions of gold particles in clusters and arrayed as monomers (13). This analysis shows that the number of GFP-tH gold particles, in a nanocluster significantly increased from ~1.8 in the control condition to ~4.5 after treatment with 100 μM indomethacin ($p < 0.05$) (Fig. 4*a*). Furthermore the fraction of GFP-tH found in clusters increased from ~50% in control to ~71% ($p < 0.05$) after treatment of cells with 100 μM indomethacin. In striking contrast, indomethacin had no effect on the fraction of GFP-tK in clusters or the average number of GFP-tK molecules per cluster (Fig. 4, *a* and *b*). These results are in exact agreement with the FLIM-FRET experiments, and suggest that the increased FRET observed is a result of both an increase in the packing density of the co-clustered fluorophores in individual clusters and an increase in the fraction of fluorophores in clusters and therefore able to undergo FRET.

Indomethacin Alters the Phase Behavior of Model Membranes—To verify that the observed effect of indomethacin is caused by a direct effect on the phospholipid bilayer, we examined the ability of indomethacin to alter membrane phase behavior in a mixed synthetic model membrane of DOPC/

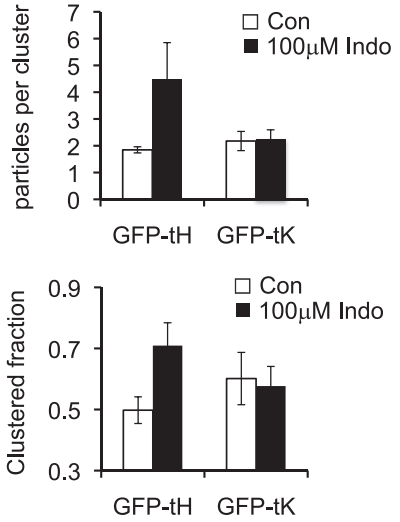

FIGURE 4. **Effect of indomethacin on nanocluster parameters of GFP-tH or GFP-tK.** The immunogold point patterns analyzed in Fig. 3 were re-interrogated to provide an estimate of the number of gold particles per cluster and the total fraction of gold particles arrayed in clusters. Note that the number of gold particles can be converted to number of GFP molecules using the known capture ratio of this GFP antisera (≈0.45, Ref. 13).

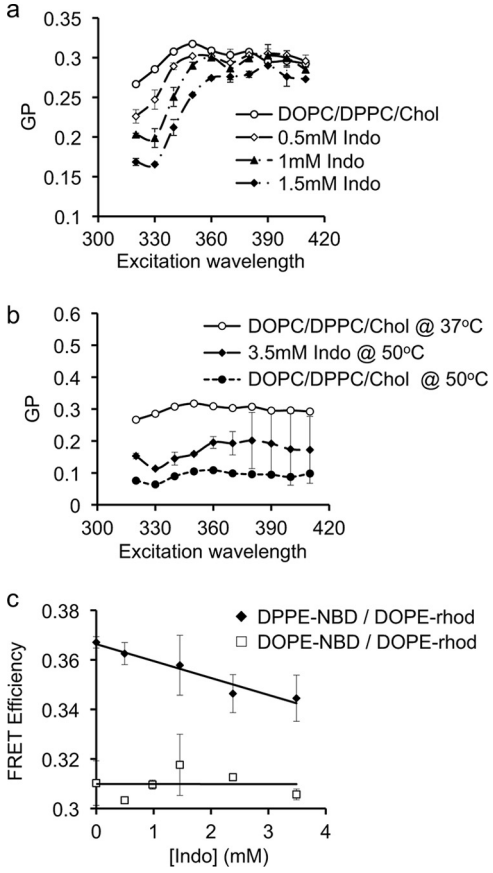

FIGURE 5. **Effect of indomethacin on the phase behavior of Laurdan in DPPC/DOPC/Chol (1:1:1).** Effect of indomethacin on Laurdan generalized polarization (GP) curves as a function of excitation wavelengths for DPPC/DOPC/Chol (1:1:1) at 37 °C (*a*) and at 50 °C (*b*). Without indomethacin, increasing temperature shifts the GP curve downward with no detectable effect on the slope of the GP curve. Addition of indomethacin at various concentrations induces a marked positive slope in the GP curves at 37 °C, indicating phase separation and the presence of co-existing phases. The slope of the GP curve is not changed by indomethacin at 50 °C. The GP data are mean ± S.D. pooled from three separate experiments. *c*, approximately 0.5 mol% of DPPE-NBD with or without DOPE-rhodamine (*solid diamonds*) or DOPE-NBD with or without DOPE-rhodamine (*open squares*) was incorporated into DPPC/DOPC/Chol (1:1:1) vesicles. Labeled liposomes were incubated in PBS containing various doses of indomethacin for 30 min before measurements. Fluorescent intensity of the donor fluorophore, DPPE-NBD or DOPE-NBD, was measured with or without acceptor fluorophore DOPE-rhodamine and FRET efficiency calculated. Data shown are mean ± S.D. pooled from 2–3 independent experiments. Indomethacin-enhanced phase separation in DPPC/DOPC/Chol (1:1:1) membrane as evidenced by decreased FRET between DPPE-NBD and DOPE-rhodamine, but had no effect on the FRET efficiency between DOPE-NBD and DOPE-rhodamine.

DPPC/Chol (1:1:1). This model membrane reflects the main lipid components found in biological plasma membrane. We measured fluorescence polarization of the membrane probe Laurdan, using the parameter of generalized polarization (GP) as a function of excitation wavelength. There are several advantages for using Laurdan: it has a large quantum yield in hydrophobic environments, such as membranes; it partitions indiscriminately into all membranes with various phase properties and it is insensitive to surface charge and solution pH (30). Two important pieces of information can be obtained from GP plotted against excitation wavelength: 1) overall polarity, where a high GP suggests a non-polar environment; and 2) the slope of the curve, which indicates phase behavior; a flat GP curve indicates gel phase, a negative slope indicates fluid phase and a positive slope indicates co-existing phases (30).

In control experiments, GP values of Laurdan in the mixed model membrane were high at 37 °C but lowered at 50 °C at all excitation wavelengths (Fig. 5, *a* and *b*). As a low GP is caused by a red shift of the emission spectrum of Laurdan when exposed to a polar environment, our data indicate that the mixed membrane is highly non-polar at 37 °C, but becomes more polar at higher temperatures. The slopes of the GP curves for the mixed membrane at all three temperatures were mostly flat. This is in a good agreement with previous studies (30, 33) and is likely due to the ability of the high levels of cholesterol (≥ 30 mol%) to broaden or abolish phase transitions (30, 33). Various concentrations of indomethacin at 37 °C shifted the GP curve down and induced a marked positive slope (Fig. 3, *a* and *b* indicating phase separation and presence of co-existing phases (30, 33). There was no effect of indomethacin on the slope of the GP curve at 50 °C, which is above the T_m of DPPC (Fig. 5*b*). Our data demonstrate that indomethacin induces phase segregation in the mixed membrane at 37 °C.

To confirm the Laurdan results, we examined the ability of indomethacin to alter the FRET efficiency between probes that segregate to separate phases. Vesicles composed of DPPC/DOPC/Chol (1:1:1) were labeled with 0.1 mol% DPPE-NBD, which favors the L_o phase, and DOPE-rhodamine, which favors the L_d phase (24). All experiments were performed at 37 °C. Without indomethacin, FRET efficiency between the probes was ~37%. Indomethacin induced a significant decrease ($p < 0.05$) in the efficiency of energy transfer between the L_o probe and the L_d probe (Fig. 5*c*), consistent with an enhancement of L_o/L_d phase separation.

To verify that the observed effect of indomethacin on FRET efficiency was not caused by changes in the inherent fluorescence properties of the probes, we labeled the mixed DOPC/DPPC/Chol membrane with DOPE-NBD, which partitions approximately equally between L_o and L_d domains with a

slightly higher preference for L_d domains (24), and DOPE-rhodamine, which prefers L_d domains. Because both probes colocalize in the L_d domains, changes in phase behavior alone should not alter the energy transfer between the probes. We found that the energy transfer between the probes was ~30% and was not changed by indomethacin exposure (Fig. 5*c*). We conclude that indomethacin does not directly interfere with the fluorescent properties of the probes and that the observed decrease in the FRET efficiency in DPPC/DOPC/Chol is caused by indomethacin-induced phase separation, in good agreement with our findings using Laurdan.

Effect of Indomethacin on L_o and L_d Domains—In a mixed DOPC/DPPC/Chol bilayer, liquid-ordered (L_o) domains are enriched in DPPC and cholesterol while liquid disordered (L_d) domains are enriched in DOPC. The segregated domains can be directly visualized in giant unilamellar vesicles (44). To better understand the underlying mechanism contributing to indomethacin-induced phase separation in a mixed DOPC/DPPC/Chol membrane, and to ascertain which component(s) in the mixed membrane indomethacin specifically targets, we examined the ability of indomethacin to alter the phase behavior of DPPC/Chol and DOPC bilayers. While these single-component and two-component membranes are intrinsically different from three-component bilayers, certain physical properties, such as fluidity and acyl chain ordering, in DPPC/Chol and DOPC bilayers are similar to those found in L_o and L_d domains, respectively, of a three-component bilayer. We therefore used these simpler systems to evaluate the potential effect of indomethacin on L_o and L_d domains in a three-component membrane. In Fig. 6*a*, we measured the effect of indomethacin on membranes comprised of DPPC/Chol (7:3) at 37 °C. Indomethacin reduced the Laurdan GP values in a dose-dependent manner, indicating increasing polarity of the bilayer. The GP curves at 37 °C displayed a marked positive slope, (Fig. 6*a*), indicating the presence of co-existing phases. Interestingly, indomethacin had no effect on the slope of the GP curve in the DPPC/Chol membrane at 50 °C (Fig. 6*b*), similar to our observation on the three-component membrane (DOPC/DPPC/Chol). Thus, indomethacin specifically targets a membrane in L_o phase and has no effect on the bilayer at a higher temperature when the membrane is in L_d phase.

To further examine the effect of indomethacin on L_d phase, we measured GP curves of Laurdan embedded in DOPC, which, with a melting temperature of −20 °C, is in L_d phase. The negative slope of the GP curve for DOPC membrane at 37 °C indicates liquid phase (Fig. 6*c*). Increasing concentrations of indomethacin at 37 °C shifted the GP curves upward but maintained the negative slope (Fig. 6*c*). The larger GP values suggest that the DOPC bilayer becomes more non-polar in the presence of indomethacin, but since the slope of the GP curve is not changed, indomethacin has no effect on the phase behavior of the fluid DOPC membrane. We conclude from these Laurdan polarization experiments at various temperatures that indomethacin induces phase separation in a membrane containing cholesterol-dependent L_o domains but has no effect on L_d domains.

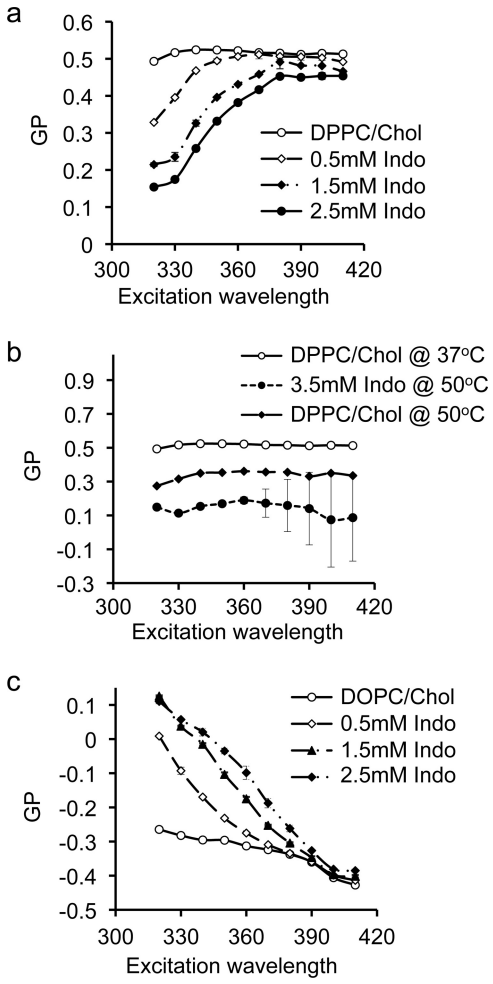

FIGURE 6. **Effect of indomethacin on general polarization of Laurdan in L_o or L_d domains.** The effect of indomethacin on GP curves of Laurdan in DPPC/Chol (30 mol%) at 37 °C (*a*) and 50 °C (*b*). The positive slope of the GP curve at 37 °C for DPPC/Chol exposed to indomethacin indicates phase co-existence. At 50 °C the effect of indomethacin on the phase behavior of DPPC/Chol is eliminated. Effect of indomethacin on general polarization of Laurdan in pure DOPC (*c*). Effect of indomethacin on GP curves of Laurdan in DOPC at 37 °C is shown. The negative slope of the GP curve indicates liquid phase. Addition of indomethacin shifted the GP curve up in a dose-dependent manner while maintaining the negative slope, indicating no effect on the phase behavior of the membrane.

DISCUSSION

Anti-inflammatory drugs, such as aspirin and indomethacin, have a wide variety of biological effects, many of which cannot be explained by their established COX inhibitory action. An interesting feature of these drugs, as well as other small bioactive molecules with wide variety of biological actions, is that they are amphiphilic and capable of intercalating into phospholipid membranes. The interactions between these amphiphiles and lipid membranes have been studied extensively in the past. It has been found that these small bioactive amphiphiles have profound effects on overall membrane integrity, mechanical, and electrostatic properties of the membrane, such as bending stiffness, lateral packing density, intramembrane dipole potential, and interfacial surface charge density (5, 45), many of which affect membrane protein aggregation, distribution and function. Hence, we propose that bioactive amphiphiles, such as indomethacin, alter membrane properties and consequen-

tially change protein function and affect cell signaling. In this study, we examined the ability of indomethacin to alter membrane heterogeneity and phase behavior, which have been demonstrated to contribute to the propagation of cell signaling events.

Using quantitative imaging of cell plasma membrane by FLIM and EM, and biophysical measurements on model synthetic membranes, we systematically characterized the ability of indomethacin to influence membrane lateral heterogeneity. The FLIM experiments demonstrated that indomethacin at various concentrations enhanced energy transfer between GFP-tH and RFP-tH, which exhibit cholesterol-dependent nanoclustering in the BHK cell plasma membrane. In contrast, indomethacin had no effect on the energy transfer between GFP-tK and RFP-tK, which exhibit cholesterol-independent nanoclustering. The EM analysis further showed that indomethacin increased the clustered fraction of GFP-tH and the packing density of GFP-tH in individual clusters. Importantly these effects on intact cells were evident at experimental concentrations of 100–150 μM, the lower values of which correspond to therapeutically relevant serum concentrations (39–43). We contend therefore that our findings are physiologically relevant.

A possible biophysical mechanism for these biological data is provided by the effect of indomethacin on a model membrane of DOPC (di18:1 PC), DPPC (di16:0 PC) and cholesterol (Chol) (1:1:1), which mimics certain properties of cell plasma membrane (11, 46–48). Our FRET and Laurdan experiments both showed that indomethacin induces L_o/L_d phase separation in this three-component bilayer. Indomethacin also induced coexisting phases in a DPPC/Chol bilayer but had no effect on the phase behavior of a pure DOPC membrane. The simplest interpretation of these data is that indomethacin specifically targets L_o domains and has no effect on L_d domains. This conclusion is further supported by our observation that indomethacin has no effect on DPPC/Chol and DOPC/DPPC/Chol bilayers at temperatures above the T_m of DPPC.

Although an effect of indomethacin or other amphiphilic drugs on membrane heterogeneity has not been reported previously, a similar effect of amphiphilic drugs has been predicted from theoretical calculations. Molecular simulations of pure DPPC suggest that amphiphilic drugs enhance thermal density fluctuation of the lipid acyl chains below T_m but have minimal effect on the density fluctuation of lipid acyl chains above T_m (9). Because chain density fluctuations in a bilayer lead to changes in fluidity and phase behavior, our findings are in agreement with these theoretical predictions. Immiscibility among various lipids contributes to phase separation in membranes (9). We propose that intercalation of highly amphiphilic indomethacin molecules enhances immiscibility between the hydrophobic ordered domains and the polar disordered domains. The hydrophobic lipids in the ordered domains pack tighter in an effort to avoid contacting the polar indomethacin molecules. This enhanced immiscibility leads to phase separation.

A critical question is to what extent these biophysical observations on model membranes can be extrapolated to biological membranes. Lateral heterogeneity in the cell plasma membrane has long been proposed (11). Local aggregation of lipids with high melting temperatures, such as DPPC, and cholesterol, with contributions from membrane proteins and the actin cytoskeleton allows the formation of dynamic L_o domains in cell membranes (11). Our results with synthetic model membranes suggest that indomethacin may stabilize this type of L_o, cholesterol dependent domain. These observations are consistent with the *in vivo* cell imaging experiments where indomethacin had a highly selectively effect on cholesterol-dependent nanoclustering, arguing for a specific effect on targeting L_o domains. As in the *in vitro* system, we speculate that the ability to induce lipid immiscibility allows indomethacin, and possibly other NSAIDs, to alter the spatiotemporal dynamics of nanoclustering in cell membranes. These dynamic changes may be reflected as increased size, or a longer lifetime of the cluster, both of which would influence the regulation of aggregation, localization, and activation of membrane-associating proteins (11). Taking these results together, we propose that indomethacin-induced changes in membrane lateral heterogeneity in turn modulate cell signaling pathways that are scaffolded on the plasma membrane.

Acknowledgment—We thank Dr. Huey W. Huang for helpful discussions.

REFERENCES

1. Tenenbaum, J. (1999) *Can J. Gastroenterol.* **13,** 119–122
2. Weggen, S., Eriksen, J. L., Das, P., Sagi, S. A., Wang, R., Pietrzik, C. U., Findlay, K. A., Smith, T. E., Murphy, M. P., Bulter, T., Kang, D. E., Marquez-Sterling, N., Golde, T. E., and Koo, E. H. (2001) *Nature* **414,** 212–216
3. Stadler, P., Armstrong, D., Margalith, D., Saraga, E., Stolte, M., Lualdi, P., Mautone, G., and Blum, A. L. (1991) *Dig. Dis. Sci.* **36,** 594–600
4. Takada, Y., Bhardwaj, A., Potdar, P., and Aggarwal, B. B. (2004) *Oncogene* **23,** 9247–9258
5. Zhou, Y., and Raphael, R. M. (2005) *Biophys. J.* **89,** 1789–1801
6. Lichtenberger, L. M., Zhou, Y., Dial, E. J., and Raphael, R. M. (2006) *J. Pharm. Pharmacol.* **58,** 1421–1428
7. Lasoner, E., and Weringa, W. D. (1990) *J. Colloid Int. Sci.* **139,** 469–478
8. Evans, E. A., and Leblond, P. F. (1972) *Nouv. Rev. Fr Hematol.* **12,** 851–860
9. Jørgensen, K., Ipsen, J. H., Mouritsen, O. G., Bennett, D., and Zuckermann, M. J. (1991) *Biochim. Biophys. Acta* **1067,** 241–253
10. Hancock, J. F. (2003) *Nat. Rev. Mol. Cell Biol.* **4,** 373–384
11. Hancock, J. F. (2006) *Nat. Rev. Mol. Cell Biol.* **7,** 456–462
12. Hancock, J. F., and Parton, R. G. (2005) *Biochem. J.* **389,** 1–11
13. Plowman, S. J., Muncke, C., Parton, R. G., and Hancock, J. F. (2005) *Proc. Natl. Acad. Sci. U.S.A.* **102,** 15500–15505
14. Shalom-Feuerstein, R., Plowman, S. J., Rotblat, B., Ariotti, N., Tian, T., Hancock, J. F., and Kloog, Y. (2008) *Cancer Res.* **68,** 6608–6616
15. Tian, T., Harding, A., Inder, K., Plowman, S., Parton, R. G., and Hancock, J. F. (2007) *Nat. Cell Biol.* **9,** 905–914
16. Abankwa, D., Gorfe, A. A., Inder, K., and Hancock, J. F. (2010) *Proc. Natl. Acad. Sci. U.S.A.* **107,** 1130–1135
17. Prior, I. A., Muncke, C., Parton, R. G., and Hancock, J. F. (2003) *J. Cell Biol.* **160,** 165–170
18. Prior, I. A., Parton, R. G., and Hancock, J. F. (2003) *Sci. STKE* **2003,** PL9
19. Hancock, J. F., and Prior, I. A. (2005) *Methods* **37,** 165–172
20. Ripley, B. D. (1977) *J. Royal Statist. Soc. B* **39,** 172–192
21. Besag, J. E. (1977) *J. Royal Statist. Soc. B* **39,** 193–195
22. Kiskowski, M. A., Hancock, J. F., and Kenworthy, A. K. (2009) *Biophys J.* **97,** 1095–1103
23. Diggle, P. J., Mateu, J., and Clough, H. E. (2000) *Adv. Appl. Prob.* **32,** 331–343
24. Silva, L. C., de Almeida, R. F., Castro, B. M., Fedorov, A., and Prieto, M.

(2007) *Biophys. J.* **92,** 502–516
25. Leidy, C., Wolkers, W. F., Jørgensen, K., Mouritsen, O. G., and Crowe, J. H. (2001) *Biophys. J.* **80,** 1819–1828
26. Parasassi, T., Conti, F., Glaser, M., and Gratton, E. (1984) *J. Biol. Chem.* **259,** 14011–14017
27. Parasassi, T., Conti, F., and Gratton, E. (1986) *Cell Mol. Biol.* **32,** 103–108
28. Parasassi, T., de Felip, E., Lepore, F., and Conti, F. (1986) *Cell Mol. Biol.* **32,** 261–266
29. Parasassi, T., De Stasio, G., d'Ubaldo, A., and Gratton, E. (1990) *Biophys. J.* **57,** 1179–1186
30. Parasassi, T., De Stasio, G., Ravagnan, G., Rusch, R. M., and Gratton, E. (1991) *Biophys. J.* **60,** 179–189
31. Parasassi, T., Di Stefano, M., Ravagnan, G., Sapora, O., and Gratton, E. (1992) *Exp. Cell Res.* **202,** 432–439
32. Parasassi, T., Gratton, E., Yu, W. M., Wilson, P., and Levi, M. (1997) *Biophys. J.* **72,** 2413–2429
33. Parasassi, T., Loiero, M., Raimondi, M., Ravagnan, G., and Gratton, E. (1993) *Biochim. Biophys. Acta* **1153,** 143–154
34. Parasassi, T., Martellucci, A., Conti, F., and Messina, B. (1984) *Cell Biochem. Funct.* **2,** 85–88
35. Parasassi, T., Sapora, O., Giusti, A. M., De Stasio, G., and Ravagnan, G. (1991) *Int. J. Radiat. Biol.* **59,** 59–69
36. Chong, P. L., and Wong, P. T. (1993) *Biochim. Biophys. Acta* **1149,** 260–266
37. Roy, S., Plowman, S., Rotblat, B., Prior, I. A., Muncke, C., Grainger, S., Parton, R. G., Henis, Y. I., Kloog, Y., and Hancock, J. F. (2005) *Mol. Cell Biol.* **25,** 6722–6733
38. Zacharias, D. A., Violin, J. D., Newton, A. C., and Tsien, R. Y. (2002) *Science* **296,** 913–916
39. Kennedy, T. G. (1985) *Biol. Reprod.* **33,** 140–146
40. Strewler, G. J., Stern, P. H., Jacobs, J. W., Eveloff, J., Klein, R. F., Leung, S. C., Rosenblatt, M., and Nissenson, R. A. (1987) *J. Clin. Invest.* **80,** 1803–1807
41. Greenberg, R. N., Murad, F., Chang, B., Robertson, D. C., and Guerrant, R. L. (1980) *Infect Immun.* **29,** 908–913
42. Kennedy, T. G. (1986) *Biol. Reprod.* **34,** 327–335
43. Jacob, M., Bjarnason, I., and Simpson, R. J. (2001) *Clin. Sci.* **101,** 493–498
44. Veatch, S. L., Polozov, I. V., Gawrisch, K., and Keller, S. L. (2004) *Biophys. J.* **86,** 2910–2922
45. Zhou, Y., Doyen, R., and Lichtenberger, L. M. (2009) *Biochim. Biophys. Acta* **1788,** 507–513
46. Ward, G. R., Huang, Y. S., Bobik, E., Xing, H. C., Mutsaers, L., Auestad, N., Montalto, M., and Wainwright, P. (1998) *J. Nutr.* **128,** 2473–2487
47. Fridriksson, E. K., Shipkova, P. A., Sheets, E. D., Holowka, D., Baird, B., and McLafferty, F. W. (1999) *Biochemistry* **38,** 8056–8063
48. Pike, L. J., Han, X., Chung, K. N., and Gross, R. W. (2002) *Biochemistry* **41,** 2075–2088